MEBT-BI-EM01-02

Thermo-Mechanical Analysis of the ESS MEBT EMU/Slit

A. R. Páramo Z. Izaola A. Vizcaíno F. Sordo I.Bustinduy

05 July 2017

Project: MEBT
Version: 2.0
Approved by: I. Bustinduy
Revised by: Z. Izaola

Change History

Rev.	Date	Author(s)	Description
0.1	2017-05-10	A. R. Páramo	First Version
0.2	2017-07-05	A. R. Páramo	Revision

Thermo-Mechanical Analysis of the ESS MEBT EMU/Slit

A. R. Páramo[1*], Z. Izaola[1], A. Vizcaíno, T. Mora[2], F. Sordo[2], I. Bustinduy[1]

[1] Accelerator/Control & Diagnostics Group, ESS-Bilbao, Spain

[2] Target Group, ESS-Bilbao, Spain

[*]Corresponding author: arparamo@essbilbao.org

Abstract.

In this report we study the thermomechanical response of the MEBT EMU/Slit during operation. We study its behaviour for the operational conditions expected during MEBT commissioning phase.

Firstly we address how the beam irradiation on the graphite plate can be withstood, operating below graphite strength limit.

Then we address operation in the steady state. We specifically address thermal contact conditions, comparing the use of stainless steel (SS) or copper (Cu) as the substrate material. Finally we chose a steel substrate as the adopted solution and study its operation with the design adopted for the EMU/Slit.

1. Introduction

This work studies the temperature, deformation and stresses that appear during operation in the EMU/Slit of the MEBT. In Figure 1 the layout of the MEBT beam instrumentation is shown.

The Emmitance Meter Unit is designed in order to measure the emittance of the proton beam in the ESS MEBT. The principles of operation of the EMU are explained in Refs. [1–4].

For the EMU/Slit, in the ESS MEBT Preliminary Design Review (PDR) [4, 5] it was shown that graphite is the chosen material to withstand irradiation. However the design of the EMU/Slit was no further analysed, in this work we define other aspects such as the substrate material, contact conditions or cooling requirements and assess that the design proposal complies with the operational requirements in the ESS MEBT.

The EMU slit is designed in order scan all the beam aperture. Since the beam envelop is ϕ40 mm, the blades width has to be >40 mm, for a total height >80 mm. For the slit, the reference values are an aperture of 100 μm and a slit thickness of 200 μm [1].

In the MEBT the beam has a nominal intensity of 62.5 mA with 3.63 MeV of energy. The EMU is designed to fulfil ESS commissioning modes [6]:

- Mode I: Fast tuning is used for steady state analysis, the average power if 16 W, for pulses of 5 μs at 14 Hz.
- Mode II: Slow Tuning is used in the transient analysis. The coating materials have to withstand ~230 kW during 50 μs with at frequency of 1 Hz, for an average power of 11 W.

As shown in Table 1, for Mode II the pulse duration is larger and we use this mode for analysis of the transient thermo-mechanical effects of irradiation in Section 3. In Mode I the average beam power is higher and we use this mode for defining the steady state operation conditions in Section 4 and 5.

The materials used in this work are a) Graphite R4550 for facing irradiation and b) Pure Copper or SS316 as substrate material. The properties of the materials are described in Appendix A: Material Properties.

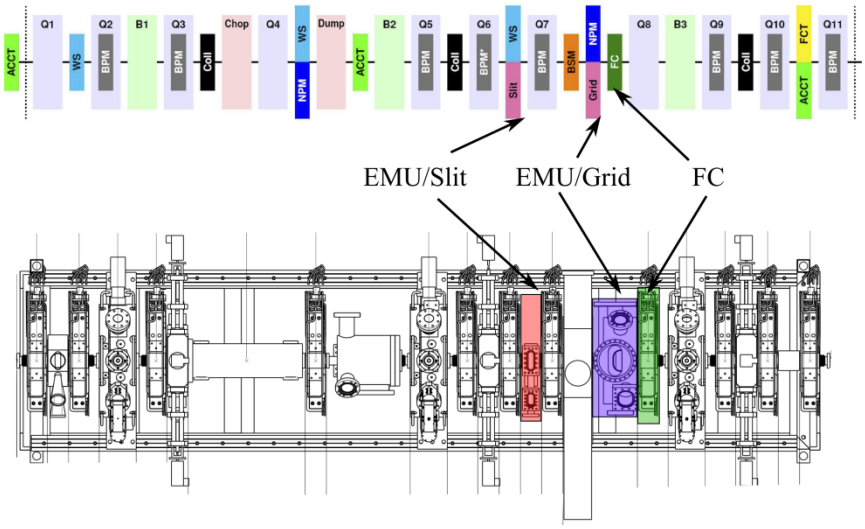

Figure 1: Top) Block diagram of the ESS-MEBT. Bottom) Layout of the ESS-MEBT.

Table 1: Beam Parameters in the EMU/Slit.

Parameter	Value		Parameter		Value	
Proton Energy	3.63	MeV	Beam Size	σ_x	3.16	mm
Intensity	62.5	mA		σ_y	3.84	mm
Mode I: Fast Tuning	5 µs - 14 Hz -16 W					
Mode II: Slow Tuning	50 µs - 1 Hz - 11 W					

2. **Design Criteria**

We can divide the analysis in two states, the *i)* transient analysis which studies the beam irradiation effects on the collector during the pulse duration, and *ii)* the steady state analysis that studies the heating of the product over operation with times of minutes.

As a first approximation, the thermo-mechanical effects can be estimated as:

$$\Delta T = \Delta T_{steady} + \Delta T_{transient} \quad (1)$$

$$\Delta \sigma = \Delta \sigma_{steady} + \Delta \sigma_{\text{transient}}$$

As we will show in the next sections (Sections 3, 4 and 5), for the graphite collector the most intense effects take place during the transient, and the steady state can be almost neglected. For the rest of components only the study of the steady state is relevant.

In order to operate with a safe limit avoiding failure, we apply a design criteria [5, 7].

- $\sigma_{Max} \leq \frac{2}{3}\sigma_{strength}$

We use Tresca criterion for graphite with a maximum stress intensity of 2/3·125=83 MPa [7, 8], and the Von Mises criteria for metals. For the material limits see Appendix A: Material Properties.

Regarding the temperature in the case of metals a general rule $T_{Max} \leq \frac{1}{3}T_{Melt}$ can be used. This general rule guarantees low operational temperatures, which is important in order to avoid temperature effects (recrystallization) that lower the structural strength of the material. In the case of graphite, the strength increases at high temperatures [8], and the temperature criterion can be relaxed.

3. Transient Analysis

3.1. Model Description

In Figure 2 we show the Ansys FEM model used in this analysis. We simulate a sample plate of 8 mm of thickness, with sides of 25 mm. The material used in this work is Graphite R4550, see Appendix A: Material Properties.

The mesh is refined in the irradiated surface in order to reproduce the Bragg Peak. Regarding mechanical boundary conditions, symmetry conditions and a fixed support in the back of the plate are applied.

Regarding thermal conditions, the analysis studies irradiation on a plate with a uniform temperature of 22 C. No cooling conditions or radiative effects are included, which results in a conservative estimation.

The thermal load is introduced from simulations in MCNPX. The proton beam is characterized by a Gaussian profile:

$$I''(x,y) = \frac{I_o}{2\pi\sigma_x\sigma_y} \cdot e^{-\frac{x^2}{2\sigma_x^2}} \cdot e^{-\frac{x^2}{2\sigma_y^2}} \quad (2)$$

We define the integrated current (I_c) as the total current flux over pulse irradiation:

$$I_c = \frac{I_o}{2\pi\sigma_x\sigma_y/\sin(\alpha)} \cdot \tau \quad (3)$$

Where I_0 is the beam current, σ_x, σ_y the beam size, α the incident angle and τ de pulse duration.

In Table 2 we show the irradiation conditions expected in the EMU for a perpendicular beam of size σ_x=0.316 cm; σ_y=0.384 cm. In order to estimate the power density (W/m^3) we multiply the current flux (A/m^2) by the stopping power (eV/m). Finally the energy deposition (J/m^3) is calculated multiplying the power density by the pulse duration.

In Figure 3 the stopping power in graphite for different incident angles is shown. We observe that the Bragg Peak for perpendicular graphite appears at ~130 μm, and that the stopping power and penetration depth scales inversely to the angle.

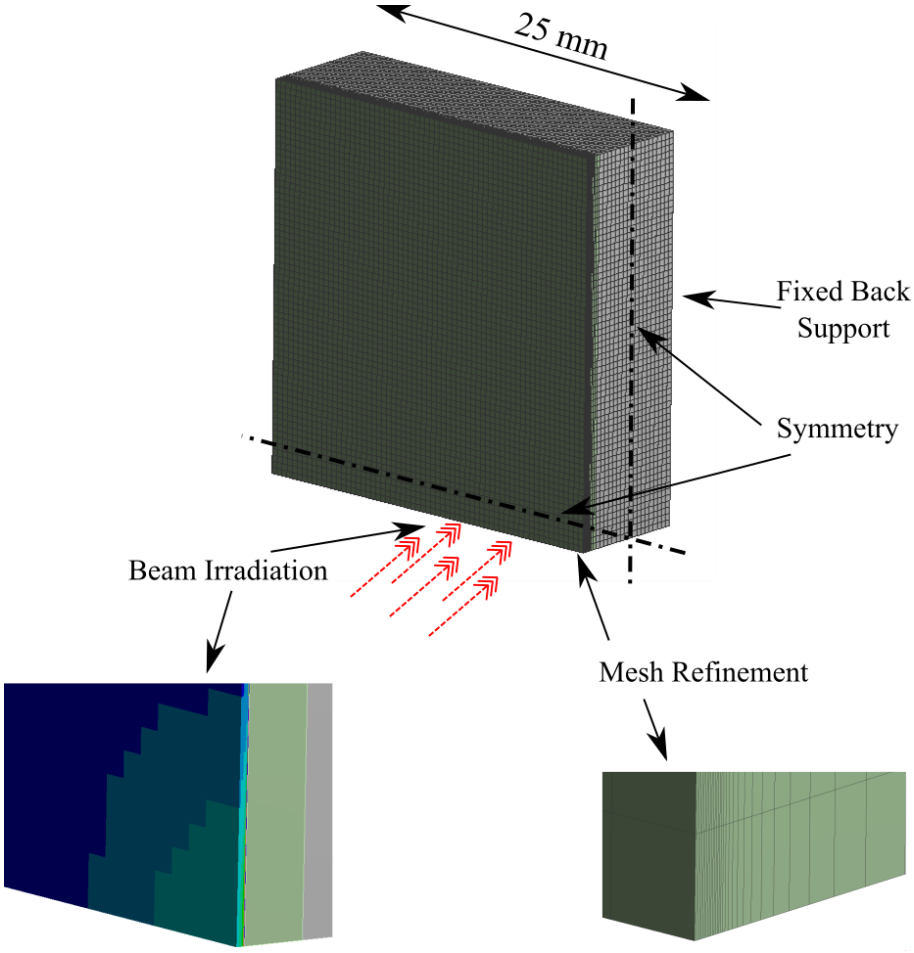

Figure 2: FEM model used in this work.

Table 2: Irradiation Conditions in perpendicularly irradiated graphite for the EMU/Slit in the commissioning mode.

Parameter	**Value**
Proton Energy (MeV)	3.63
Beam Current (mA)	62.5
Pulse duration (μs)	50
Pulse Energy (J)	11
Peak Power (kW)	227
Beam Sigma (cm)	σ_x=0.316 cm σ_y=0.384 cm
Beam Spot (cm^2)	0.76
Beam Current (mA/cm^2)	159
Integrated Current (μC/cm^2)	4.1
Stopping Power (MeV/cm)	775
Energy Deposition (MW/cm^3)	64
Energy Deposition (kJ/cm^3)	3.2

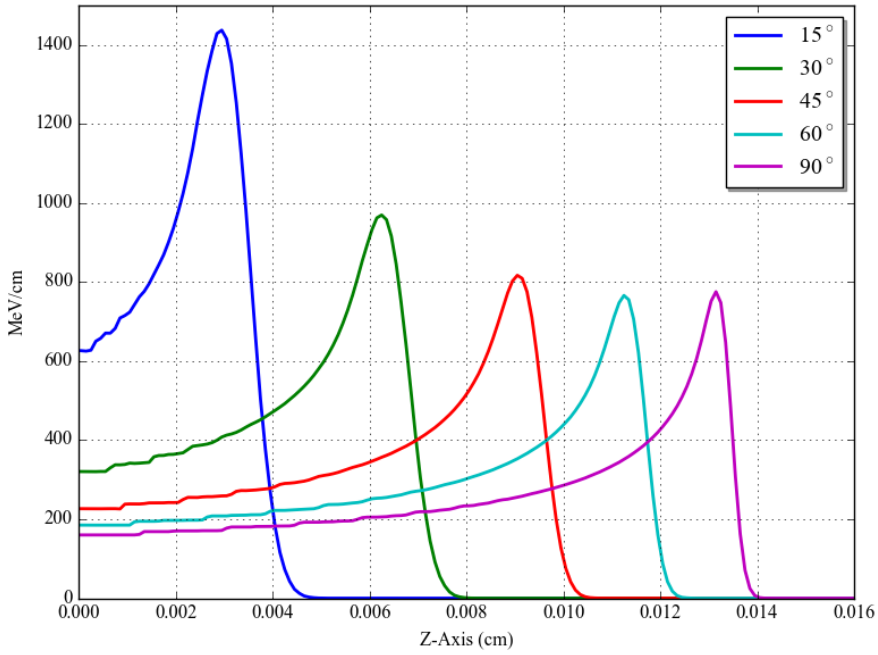

Figure 3: Stopping power for 3.63 MeV protons in Graphite as function of the incident angle.

3.2. **Thermo-Mechanical Results of Beam Irradiation**

In this section we show the results for the beam conditions in the EMU/Slit. For this purpose we study the nominal conditions with a beam energy of 3.63 MeV, intensity of 62.5 mA, and pulse duration of 50 μs. For the EMU/Slit we study a beam spot of σ_x=3.16 mm and σ_y=3.84 mm. In order to observe the deformations in the EMU/Slit, we slightly modify the model described in Section 3.1, removing the vertical symmetry, having a free surface for the aperture of the EMU/Slit.

In Figure 4 we show the temperature stresses and deformations of the EMU/Slit. The maximum temperature corresponds to the Bragg peak, at ~130 μm below the surface.

Regarding the stresses, compression (σ_3) appears at the irradiated zone. The maximum compression stresses appear in the Bragg peak. Regarding the compression stresses (σ_3) we operate always below the design limit, at $\sigma_{Int}/\sigma_{Lim.}$~35%. At depths higher than the irradiated zone (>150 μm), a tensile zone (σ_1) appears. The tensile zone is defined by boundary conditions and for the EMU is up 7 MPa. The stress intensity (σ_{Int}) is therefore dominated by compression stresses, which are much higher than tensile stresses. Regarding the deformations, we observe that the EMU/Slit, the total aperture will close ~2 μm after each beam irradiation.

In Table 3 we summarize the main thermo-mechanical conditions in the EMU/Slit.

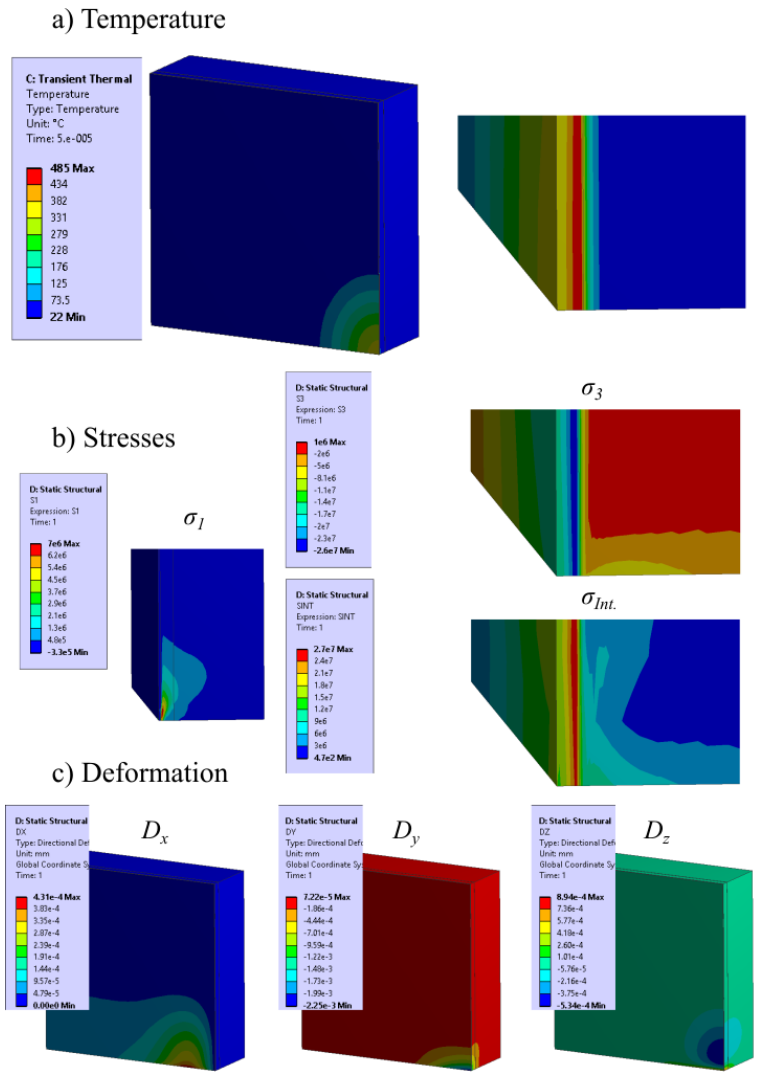

Figure 4: Temperature, stresses and deformations after beam irradiation (50 µs) in the EMU/Slit.

Table 3: Main thermo-mechanical conditions after beam irradiation (50 µm) in the EMU/Slit.

Case	***I''* (µC/cm²)**	**ΔT (K)**	**σ_1 (MPa)**	**σ_3 (MPa)**	**σ_{Int} (MPa)**	**$\sigma_{Int}/\sigma_{Lim.}$**	**Max. Def. (µm)**
EMU/Slit	4.1	463	7.6	-26	27	32%	2.3

4. **Preliminary Steady State Analysis**

In this section we study a simplified geometry of the EMU/Slit. With this simple model we specifically address the use of copper or steel as the substrate material and the contact requirements. On one side copper offers excellent thermal properties but a more difficult fabrication process, while the use of steel results in only acceptable thermal properties but a simple fabrication process. From the analysis we select a steel substrate with contact forces of 250 N as the design proposal.

4.1. **Model Description**

In Table 4 the main dimensions of the FEM model are shown, and in Figure 5 the geometry is shown. The EMU/Slit has a total width of 56 mm, having 8 mm at each blade side for pressed contact. For the height we use 100 mm.

For the refrigeration system we use a channel of 2 mm radius. Assuming cooling conditions with water at 300 K and flowing at ~1 m/s a film coefficient of h=5000 $Wm^{-2}K^{-1}$ is applied in the model [9] , see also Appendix C: Cooling Requirements. For the thermal conditions we have not included radiative effects.

For the support of the EMU/Slit we apply null node displacement in the upper part of the model, corresponding to the joining with the actuators. We also apply symmetry conditions since only half of the EMU/Slit is simulated.

A border contact between graphite and substrate is imposed in the lateral of the slits through a contact force, see Figure 6. Structural simulations show that effective contact is only attained in the contact surface. In the centre, the Graphite and substrate surface will not be in contact. We apply a contact model with a friction coefficient of 0.1. This allows the graphite to slide over the substrate and accommodate thermal expansions.

The thermal contact is defined by the model described in Appendix B: Thermal Contact Model. We have a thermal conductance of 0.0146 $WN^{-1}K^{-1}$ for a Gr-Cu contact and 0.0019 $WN^{-1}K^{-1}$ for Gr-Steel Contact.

The thermal load has been calculated introducing beam parameters (see Table 1) in a MCNPX model. The Bragg Peak for a 3.63 MeV proton beam in graphite is situated at ~130 μm and becomes null at ~140 μm [5]. Since we are studying effects in the steady regime we homogenize the heat source in a mesh element of 140 μm. The beam size is defined by σ_x = 3.157 mm and σ_y=3.835 mm. In Figure 7 we show the heat load used in this work.

Table 4: FEM Model of the EMU/Slit: materials and main dimensions.

Parameter	Value	Parameter	Value
Coating Material	Graphite	Graphite Thickness	3 mm
Substrate Material	Steel/Copper	Substrate Thickness	10 mm
		Contact Border	8 mm
Water Channel Radius	2 mm	Slit Blade Width	56 mm
Film Coefficient	5000 $Wm^{-2}K^{-1}$	Slit Blade Height	100 mm
Water Temperature	300 K		

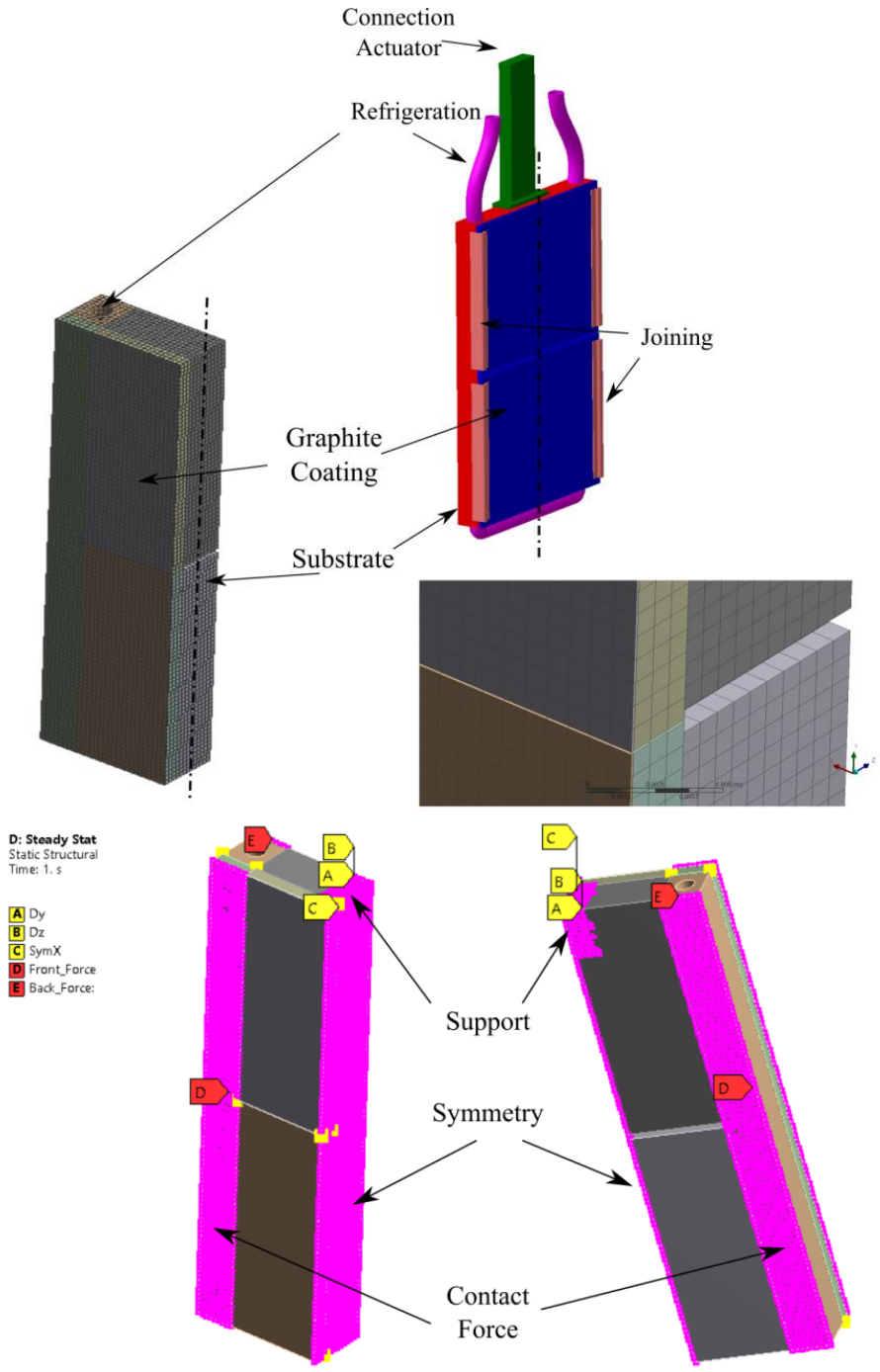

Figure 5: FEM model of the EMU/Slit. Top) Geometry and mesh description. Bottom) Boundary conditions.

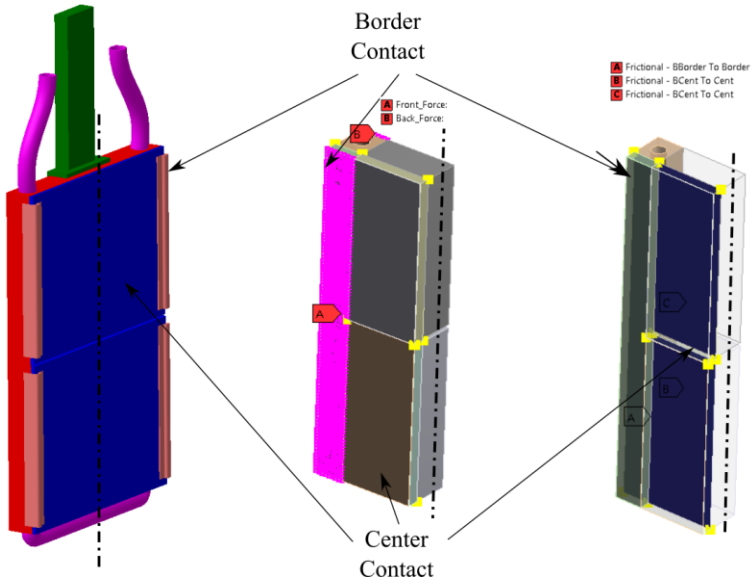

Figure 6: Contact Model of the FEM Model

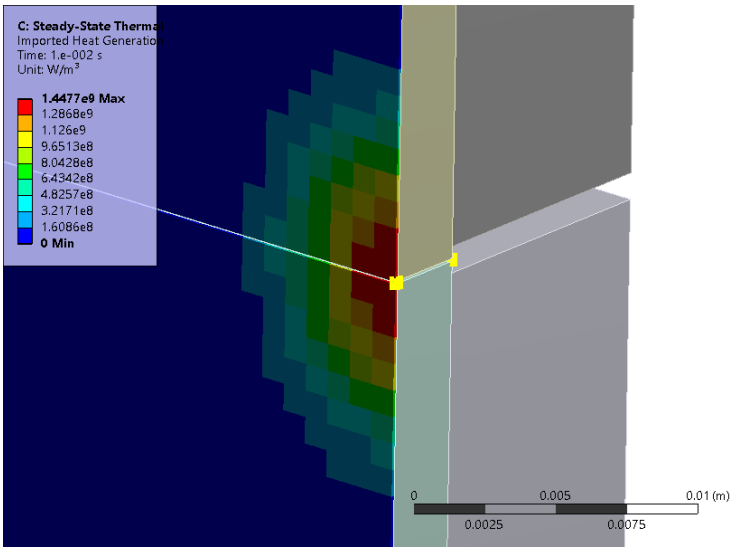

Figure 7: Thermal Load of the FEM Model as imported from the MCNPX simulations.

4.2. **Contact Force Parametric Analysis**

A temperature control is important is order to minimize deformation obtaining higher accuracies in the system. For this purpose we study the thermomechanical behaviour as function of the contact force. We aim for a design where the maximum temperature in the steady state is <100 K and maximum deformation < 20 μm in order control the aperture and position of the slit during operation.

In Figure 8 we show the temperature variation as function of the contact force. In total the temperature in the steady state is defined by a) the temperature gradient in the graphite b) temperature gap in the contact region, c) temperature gradient in the substrate and d) temperature gap with the coolant. The temperature gradient in the graphite is ~25 K. The temperature gap in the graphite-substrate contact is represented by the dashes lines in Figure 8. We observe how for copper the contact temperature gap is low (<30 K in all cases). However for contact with SS larger forces need to be applied, and the contact gap gets below 50 K for forces higher than 250 N. The temperature gradient in the substrate is low in both cases < 5 K. Finally, the temperature gap with the coolant is ~1 K.

In Figure 9 we show the deformations of the graphite slit as function of the contact force. It is important to remark that since the graphite slides over the substrate, the thermal deformation is accommodated and the slit aperture remains almost constant. Due to the temperature gradient expansion the slit only closes ~2 μm for the different cases, due to the transient pulse (See Section 3), at the end of the pulse the slit would close approximately another 2-5 μm.

Regarding deformation in the upper and lower parts of the slit (see Figure 11). For copper, the deformation is always below 20 μm, while in the case of a steel substrate contact forces > 250 N should be applied.

From these results contact forces ~50 N in case of a copper substrate and 250 N in the case of a steel substrate are recommended.

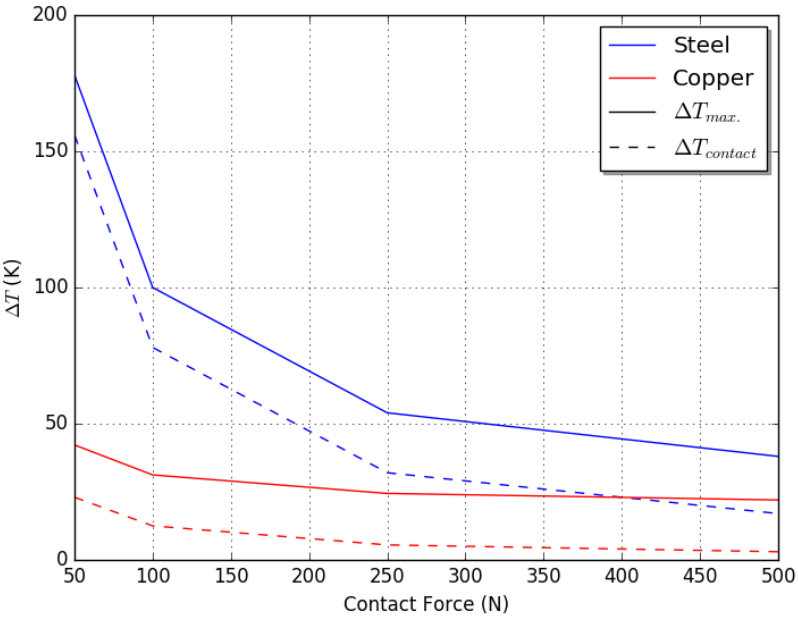

Figure 8: Temperature variation as function of the contact force.

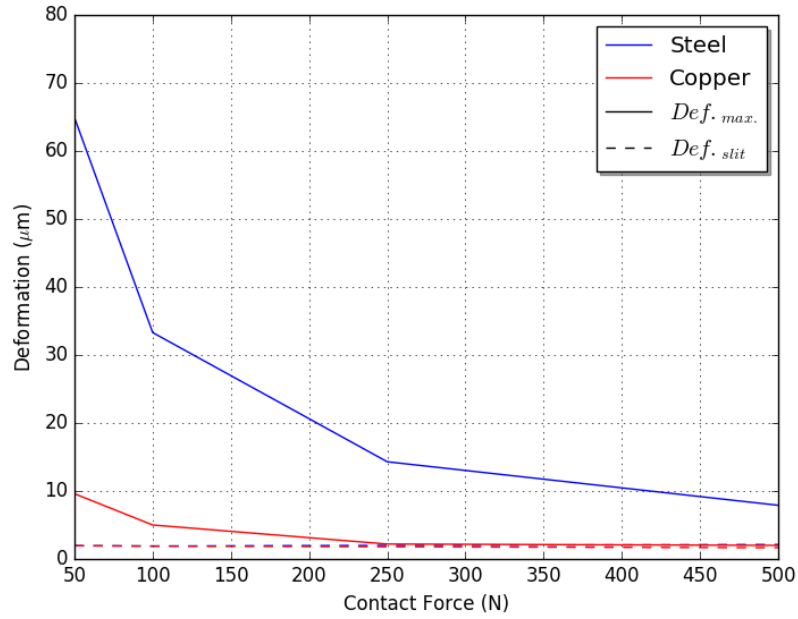

Figure 9: Graphite and Slit deformation as function of the contact force.

4.3. **Thermo-Mechanical Results**

Next we show the results for a) copper substrate with a contact force of 50 N and b) steel substrate with a contact force of 250 N.

In Figure 10 the maximum temperature in the graphite after beginning of operation is shown. It is observed that the steady state is attained in 200-400 s, which is more or less the time of operation of the EMU/Slit in order to scan the proton beam.

In Figure 11 the temperature, deformation and stresses and for cases with copper and steel substrate are shown. The temperature and deformation where already discussed in the previous sections. Regarding the stresses we observe that in the graphite they have a maximum of σ_1=0.3 MPa and a minimum of σ_3=-3.5 MPa. This stresses are attained in the slit aperture border, therefore rounded finishing is recommended. In any case this level of stresses is lower than to the stresses attained during the transient [5].

Figure 12 shows contact pressure, a maximum of 0.25 MPa is attained in the case of a contact force of 250 N. It is important to note that in the centre of the slit no contact is observed. Effective contact only appears in the borders, where the force is applied.

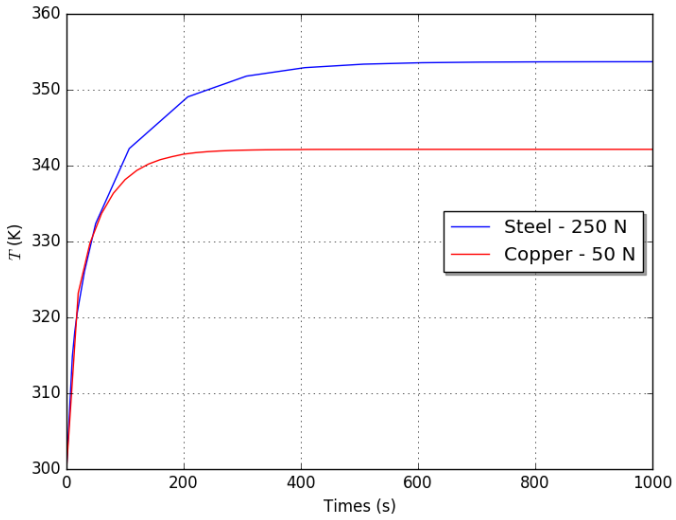

Figure 10: Temperature transient after the start-up.

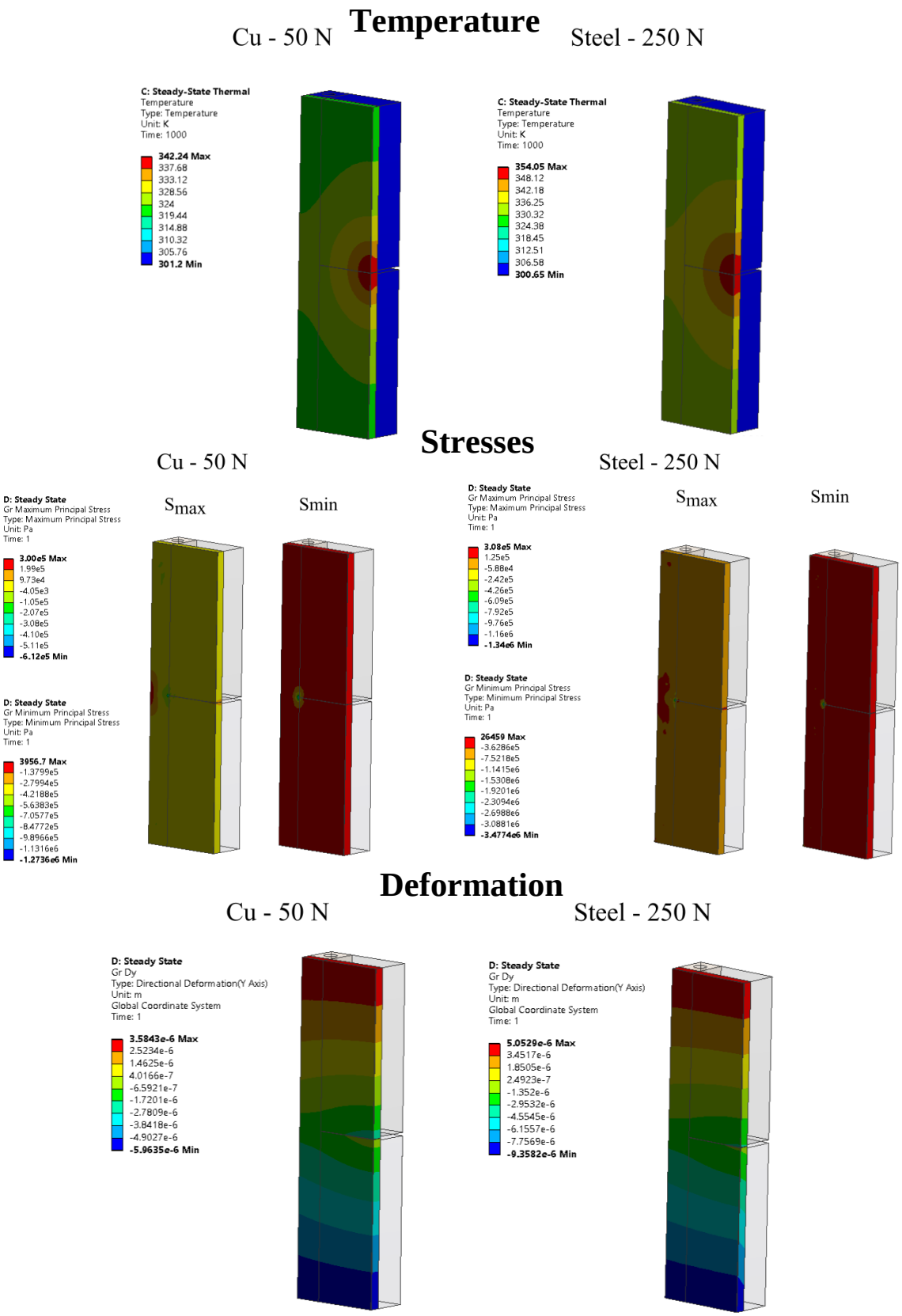

Figure 11: Temperature, stresses, deformation contours in the EMU/Slit. left) Cu substrate with a contact force of 50 N and right) Steel substrate with a contact force of 250 N.

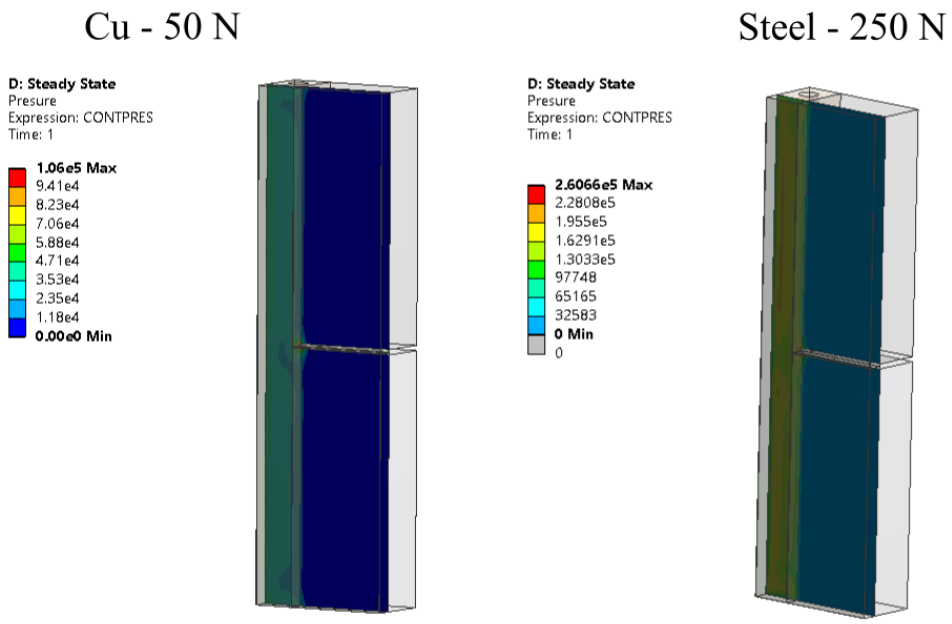

Figure 12: Contact pressure contours for left) Cu substrate with a contact force of 50 N and right) Steel substrate with a contact force of 250 N.

5. **Final Geometry Steady State Analysis**

In this section we perform a thermomechanical analysis on the final design of the EMU/Slit. From the previous sections we are able to select the main parameters of the design, such as graphite as the coating material, steel as the substrate and a joining force of 250 N.

We update the geometry of the model, and assessing that the proposed design fulfils the operational requirements for the EMU/Slit.

5.1. **Model Description**

In Table 5 the main dimensions of the FEM model are shown, and in Figure 13 the geometry is shown.

For the refrigeration system we use a channel of 2 mm radius. Assuming cooling conditions with water at 300 K and flowing at ~1 m/s a film coefficient of h=5000 $Wm^{-2}K^{-1}$ is applied in the model [9] , see also Appendix C: Cooling Requirements. For the thermal conditions we have not included radiative effects.

For the support of the EMU/Slit we apply null node displacement in the upper part of the model, corresponding to the joining with the actuators. We also apply symmetry conditions since only half of the EMU/Slit is simulated.

A border contact between a washer plate, the graphite and substrate is imposed in the lateral of the slits through a contact force, see Figure 13. Structural simulations show that effective contact is only attained in the contact surface. In the centre, the Graphite and substrate surface will not be in contact. We apply a contact model with a friction coefficient of 0.1. This allows the graphite to slide over the substrate and accommodate thermal expansions.

The thermal contact is defined by the model described in Appendix B: Thermal Contact Model. We have a thermal conductance 0.0019 $WN^{-1}K^{-1}$ for Gr-Steel Contact. A total force of 250 N (or 31 N per screw) should be applied on a contact surface of ~10 cm^2 leading to a contact conductance of ~460 W/m^2K.

The thermal load has been calculated as a surface flux[1]. The beam parameters are (see Table 1) a current of 62.5 mA, proton energy of 3.63 MeV a beam size is defined by σ_x = 3.157 mm and σ_y=3.835 mm and a mode operation of 5 μs and 14 Hz for an average heat load of 16 W.

[1] Local effects of energy deposition affect only during the pulse transient as studied in in Section 3. For the analysis of the steady state operation the surface flux approach offers a more simple approach for the characterization of beam irradiation.

Table 5: FEM Model of the EMU/Slit: materials and main dimensions.

Parameter	Value	Parameter	Value
Coating Material	Graphite	Graphite Thickness	3 mm
Substrate Material	Steel/Copper	Substrate Thickness	12 mm
		Washer Plate Width	7 mm
Water Channel Radius	2 mm	Slit Blade Width	54 mm
Film Coefficient	5000 $Wm^{-2}K^{-1}$	Slit Blade Height	80 mm
Water Temperature	300 K		
Gr-Steel Force	250 N		
Gr-Steel Conductance	0.0019 W/NK 460 W/m^2K		

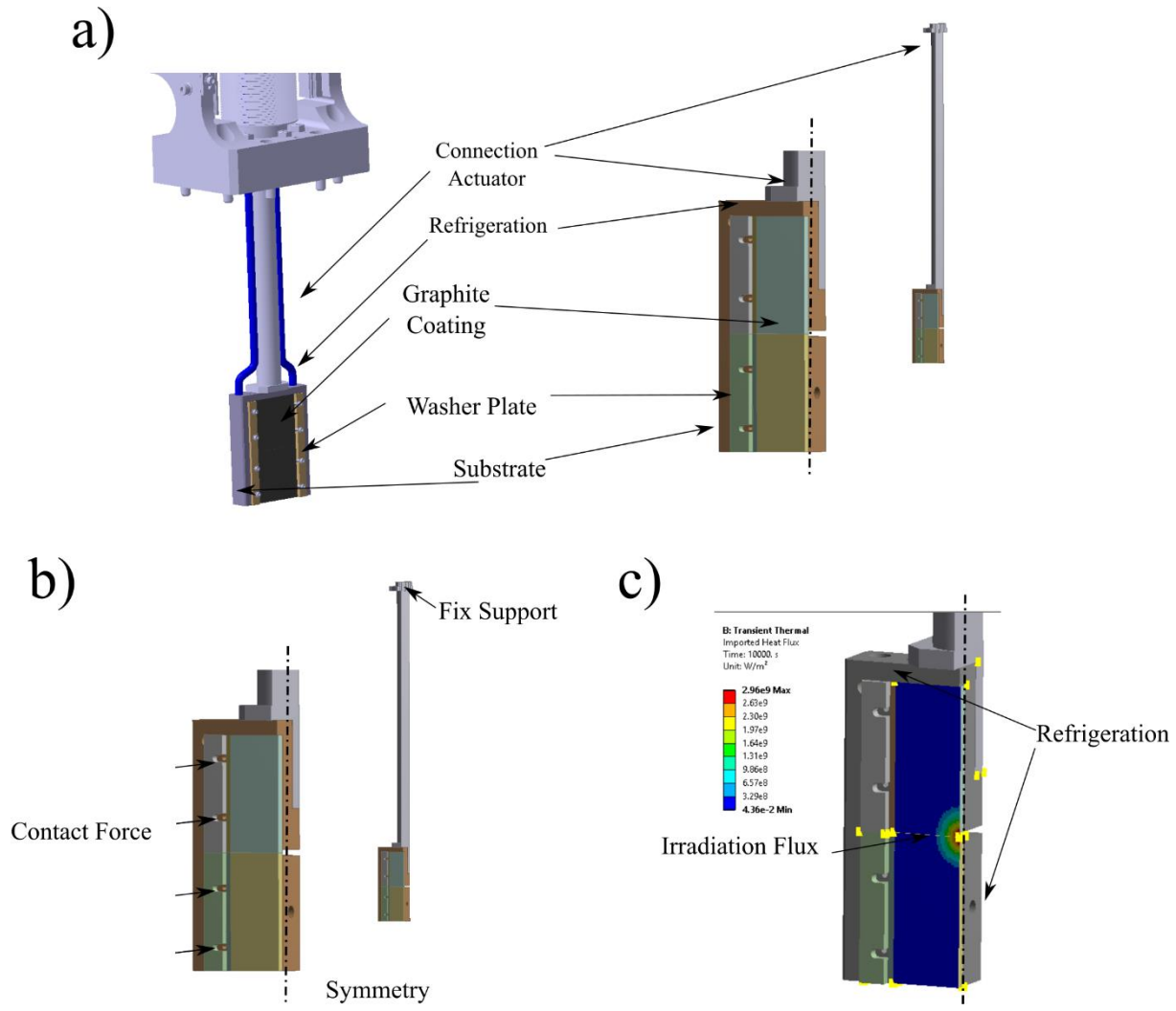

Figure 13: FEM model of the EMU/Slit. a) CAD Model and simplified FEM model. b) Mechanical and c) Thermal boundary conditions.

5.2. **Thermo-Mechanical Results**

A temperature control is important in order to minimize deformation obtaining higher accuracies in the system. We aim for a design where the maximum temperature in the steady state is <100 K and maximum deformation < 20 μm in order control the aperture and position of the slit during operation.

In Figure 14 the maximum temperature in the graphite and in the steel body after beginning of operation is shown. It is observed that the steady state is attained in around 400 s, which is more or less the time of operation of the EMU/Slit in order to scan the proton beam. The graphite attains a maximum temperature of ~360K and the minimum ~335 K, meaning a temperature gradient of ~25 K in the graphite. The maximum temperature in the steel substrate is ~310 K. The temperature gap in the contact region between the graphite and the body is around 25 K.

In Figure 15 the temperature, stresses, deformation and contact pressure in the steady state regime are shown. Regarding the stresses, they are much lower than the material limits for steel and graphite, and the structural stability is guaranteed. Regarding the deformations, it is important to focus on the graphite, and the deformations in the slit. The maximum deformation in the graphite is ~17 μm in the lower part of the plate. However if we focus only on the slit closure is just around 2 μm. Due to the temperature gradient expansion the slit only closes ~2 μm for the different cases, due to the transient pulse (See Section 3), at the end of the pulse the slit would close approximately another 2 μm, for a total closure of ~4 μm. Therefore the thermal deformations in the slit are low and correct operation is expected.

Since the contact for graphite/steel can lead to local concentration of stresses we also study the contact pressure. profile. The graphite is pressed to the steel through washer plate which is tightened by a screw. The use of the washer plate is included to create a homogeneous pressure in the graphite contact interfaces. In the graphite-washer interface a pressure of 1.5 MPa appears, and in the graphite-substrate, a pressure 0.8 MPa is attained. We observe that although the contact pressures is higher near the screwed joins, it is distributed over a larger region of the graphite-body contact, which would guarantee good contact conditions for the dissipation of the heat load.

In **Error! Reference source not found.** we summarize the conditions of operation for the proposed solutions for the EMU/Slit.

Table 6: Main thermo-mechanical conditions in the graphite plate of the EMU/Slit, with contact forces of 250 N.

Case	ΔT **(ºC)**	σ_1 **(MPa)**	σ_3 **(MPa)**	σ_{Int} **(MPa)**	$\sigma_{Int}/\sigma_{Lim.}$	**Slit. Def. (μm)**
Initial	17	0	0	0	0	0
Steady	57	0.75	-1.5	1.5	2 %	2
Transient	463	7.6	-26	27	32%	2.3
Total (Init + Steady + Transient)	**537**	**7.6**	**-26**	**27**	**32%**	**4.3**

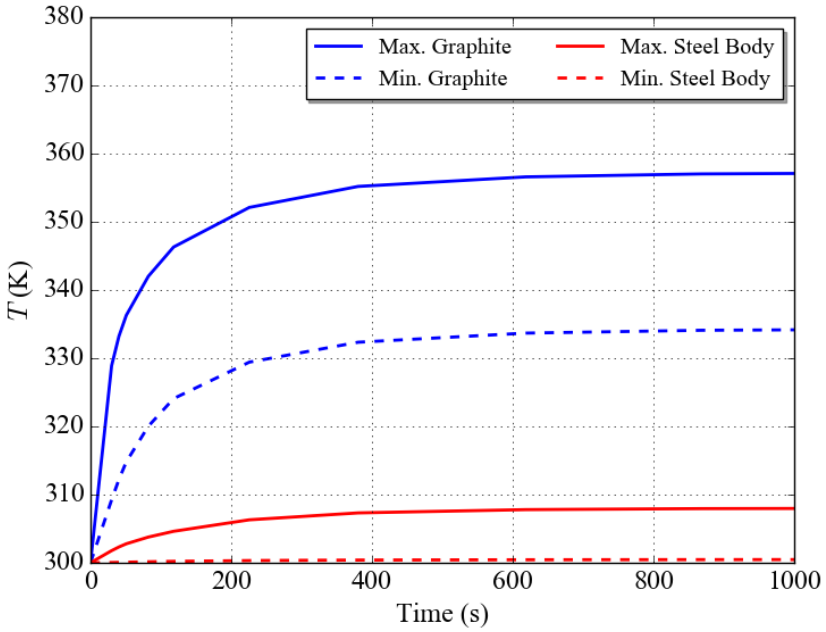

Figure 14: Temperature transient after the start-up.

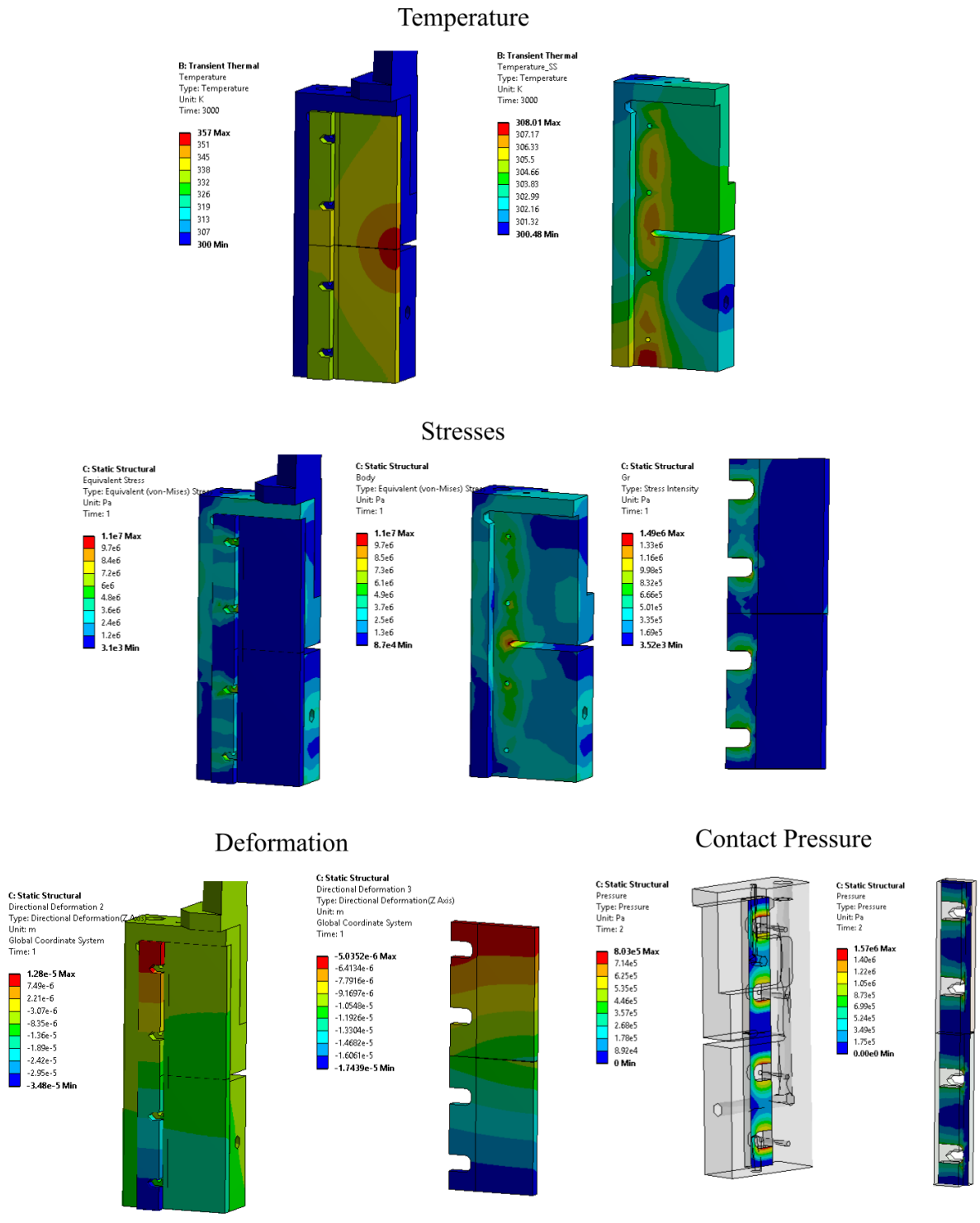

Figure 15: Temperature, stress, deformation and contact pressure contours. Please note that the scales of the figures are different, displaying different components of the EMU/Slit.

6. **Conclusions**

In this work we study thermo-mechanical effects for operation in the EMU/Slit of the MEBT line. We study its behaviour for the operational conditions expected during MEBT commissioning phase. First we study beam irradiation of the graphite (Section 3) collector, then we do a preliminary analysis on the EMU/Slit, analysing the effect of the body material and the contact force requirements (Section 4) and finally we study the proposed design of the EMU/Slit.

The beam irradiation transient is characterized by material heating and expansion which leads to compressive stresses during pulse irradiation. The maximum temperature and stresses take place in the Bragg Peak, and depend on the energy deposition and heat diffusion.

We study the behaviour during the irradiation pulse, studying how the maximum temperatures and stresses in the irradiated graphite are lower than the design limits. In Table 6 we summarize the main results of the work. We observe how for the EMU/Slit we operate at ~30 % of the design limit.

For the steady state we first study the substrate material and the required contact force, concluding that a steel substrate with contact forces of 250 N would guarantee correct operation. Finally we study this solution with the final design of the EMU/Slit.

Appendix A: Material Properties

In this model we use Graphite R4550 with material properties obtained from Linac 4 Cern Group, and reported in Refs. [5, 7], we obtain its hardness from Ref. [8]. For Steel we use SS316L properties reported in Ref. [10] with strength limits from Ref. [11] and microhardness from Ref. [12]. For copper we use pure copper properties reported in Ref. [10] with strength limits from Ref. [13].

The material properties of the materials used in the work are summarized in Table 7.

Table 7: Material properties for Graphite R4550 [5, 7, 8] , SS316 [10–12], pure copper [10, 13].

Mat. Limit	**Graphite**	**Steel**	**Copper**
Max. Temp. (K)	3773	1700	1357
Ult. Tensile Strength (MPa)	40	450	209
Ult. Comp. Strength (MPa)	125		
Yield Strength (MPa)	-	170	33
Young Modulus (GPa)	11.7	200	125
Poisson Coefficient	0.15	0.3	0.343
Thermal Conductivity, at 300 K (W $m^{-1}K^{-1}$)	103	14	398
Density, at 300 K (kg m^{-3})	1800	7930	8930
Specific Heat, at 300 K (J kg^{-1} K^{-1})	824	472	385
Coefficient ff thermal expansion, at 300 K (μm m^{-1} K^{-1})	4	15	16

Appendix B: Thermal Contact Model

In this section we describe the thermal contact model used in this work.

We apply the model to the contact regions. In the regions where not mechanical contact is expected we assume adiabatic conditions.

In our case we model conforming rough contacts, where the contact thermal conductance (h_c) is dependent conductivity (k), roughness (σ/m) and micro-hardness (H_c) of contact materials. For the analysis we use Yovanovich's model[12, 14–17]:

$$h_c \cdot \frac{\sigma_c/m_c}{k_c} = 1.25 \cdot \left(\frac{P}{H_c}\right)^{0.95} \quad (4)$$

Since we want to study the thermal contact as function of the contact force we have linearized the previous equation. This results in a conservative estimation of the contact conductance as function of the force, obtaining h_c/P in $WN^{-1}K^{-1}$.

$$h_c \cdot \frac{\sigma_c/m_c}{k_c} \lesssim 1.25 \cdot \left(\frac{P}{H_c}\right) \quad (5)$$

$$\frac{h_c}{P} \lesssim 1.25 \cdot \frac{k_c}{\sigma_c/m_c} \cdot \frac{1}{H_c}$$

Where k_c is the contact conductivity that can be estimated as the harmonic mean of both materials [14, 15]:

$$k_c = \frac{k_1 \cdot k_2}{(k_1 + k_2)/2} \quad (6)$$

The surface roughness, σ, and the asperity slope, m, can be estimated as [15]:

$$m = 1.52 \cdot \left(\frac{\sigma}{1\mu m}\right)^{0.4} \quad (7)$$

In order to calculate the contact roughness $\sigma_c^2 = \sigma_1^2 + \sigma_2^2$ and $m_c^2 = m_1^2 + m_2^2$ [14, 15].

For the microhardness H_c the softer of the two materials is taken [12, 14].

In the case of metals, the microhardness H_c can be can be calculated as [12, 16].

$$H_c = C_1 \cdot \left(1.62 \cdot 10^6 \cdot \frac{\sigma}{m}\right)^{C_2} \quad (8)$$

Where C_1 and C_2 are the Microhardness Vickers coefficients. C_2 ~ -0.26 for most materials [12]. C_1=6906 MPa for steel [12]. Since for metals hardness is proportional to the tensile strength, $H \sim 3\sigma_u$ [15, 18, 19], we estimate C_1 for copper as 3207 MPa.

In the case of non-metals (alumina, graphite), hardness is larger than the tensile stress ($H \gg 3\sigma_u$). Therefefore in order to calculate C_1 we will extrapolate from macro-hardness using Eq. (8), and assuming the curve intersects with macrohardness at σ =700 μm [2]. For graphite we have a macrohardness of $90HR_{5/100}$ [8], which can be approximated to ~737 MPa [20] and from which we obtain C_1=3700 MPa. In Table 8 we summarize the macro and micro-hardness parameters used in this model.

In Ref. [7] a contact conductance for Gr-Cu of $\boldsymbol{h_c/P}$**~0.0145 WN^{-1}K^{-1}** , which is in agreement with our model if we assume a roughness σ = 1.6 μm.

Under the conditions assumed in our model, for Gr-Steel we estimate a contact conductance h_c/P~0.002 WN^{-1}K^{-1}. This is 7 times lower than for Gr-Cu and therefore Gr-Steel will need of contact forces 7 times higher than Gr-Cu in order to have a similar thermal behaviour.

In Table 9 we show the thermal conductance and resistance for different contact pairs in our model. It is important to point out that these values correspond to the model described in this section, which depends on many parameters (material hardness, roughness, conductivity, plastic contact behaviour, etc). We have compared our model to the Gr-Cu contact given in Ref. [7], for the rest of contact pairs the results should give qualitative trends of the contact behaviour as function of the materials.

Table 8: Hardness parameters of the model.

	Graphite	**Steel**	**Copper**
Macrohardness (MPa)	713	1350	627
Microhardness, C_1 (MPa)	3700	6906	3207

Table 9: Thermal Contact Conductance and Resistance of the model.

	Conductance (WN^{-1}K^{-1})	**Resistance (KNW^{-1})**
Gr-Cu	0.0146	69
Gr-SS	0.0019	517

[2] This is the roughness for microhardness intersection with macrohardness that appears for our model in the case of metals.

Appendix C: Cooling Requirements

In this document, film coefficients of ~5000 W/m^{2}K are specified. For the design of the FC channels of 4 mm of inner diameter will be most probably used.

In order to estimate the film coefficient we use Colburn equation [9]:

$$Nu = 0.023 \cdot Re_D^{4/5} \cdot \mathrm{Pr}^{1/3} \quad (9)$$

Where $Nu = h \cdot D/k$ is the Nusselt number, *Re* the Reynolds number and *Pr* the Prandtl number.

The pressure losses can be calculated as:

$$\Delta P = \frac{1}{2}\left(f\frac{L}{D} + K\right) \cdot \rho \cdot v^2 \quad (10)$$

Where *f* is the friction factor, *L* the equivalent pipe length, *D* the pipe diameterρ the fluid density, *K* the singular losses and *v* the speed.

In order to have a quick estimation of the friction factor we can use explicit formulations such Haaland [21]:

$$\frac{1}{f^{1/2}} = -1.8 \cdot \log\left(\frac{6.9}{Re_D} + \left(\frac{\epsilon/D}{3.7}\right)^{1.11}\right) \quad (11)$$

Where *f* is the friction factor, *Re* the reynolds number, ϵ is the pipe roughness and *D* the pipe diameter.

In order to have a preliminary estimation we can assume a roughness of ϵ=100 μm, tubing length of 2 m and singular losses K~20 [21].

In Table 10 we show the main heat transfer parameters. We observe that in order to obtain a film coefficient ~5000 W/m^{2}K in a channel of ϕ 4 mm we need water flowing at 1 m/s or ~0.75 l/min. For the pressure losses for this system, and we observe that they are in the range of 0.2 bars.

Table 10: Main parameters for the heat transfer and pressure losses of a water cooled channel.

Parameter	Value	Unit
ID	4	mm
v	1	m/s
Q	1.75	l/min
Re	3988	
Nu	33	
H	5008	$W/m^2 K$
f	0.06	
L	2	m
$\Delta P_{friction}$	15230	Pa
K	20	
$\Delta P_{singular}$	9899	Pa
ΔP	25219	Pa
	0.25	Bar

Appendix D: Screw Tightening

In this work we conclude that contact forces of ~250 N are required for the EMU/Slit. In the EMU/Slitthe design includes 8 screws, therefore each screw requires 31 N.

As a general approximation, the tightening torque depends on the pitch of the screw and on the friction in the thread and the screw head. As a general approximation, the torque can be calculated as [15]:

$$T = \left(\frac{p \cdot F}{2\pi} + 0.58 \cdot \mu \cdot d_2 + \mu_b \cdot r_m\right) \qquad (12)$$

Where F is the contact force, p is the screw pitch, d_2 is the screw mean diameter, r_m is the mean radius in the screw head, μ is the friction factor in the thread and μ_b the friction fator in the head.

Therefore the required torque depends a lot on the screws chosen for the design. The proposed design for the FC uses ISO 4762 M3 screws [3]. For these screws p=0.4 mm, d=2 mm, r_m =1.45 mm. Standard friction coefficients for steel-steel contacts[4] are slightly below 1, so we can assume μ=μ_b=1. With the previous assumptions a tightening torque of 0.08 Nm would be necessary.

The recommended seating torque for ISO 4762 screws is ~0.5 Nm for M2 [5]. Fastening with these torques would result in contact pressures ~5 MPa, which is lower than the graphite strengths. Therefore fastening the screws with the recommended torque will result in adecuate contact conditions.

Since the correspondence of screw torque and force depends greatly on geometry and friction, a calibration of the torque-force relation can be done using disc spring. For example disc springs DIN 2093[6] offer contact forces of 50-100 N.

[3] http://www.fasteners.eu/standards/ISO/4762/

[4] http://www.engineeringtoolbox.com/friction-coefficients-d_778.html

[5] http://fullerfasteners.com/tech/torque-information/

[6] http://schnorr.com/download/schnorr-product-range/?wpdmdl=94

Appendix E: Comparison of ESS MEBT and Linac 4 EMU

In this Appendix we compare the operational conditions in the ESS MEBT EMU/Slit and in the Linac 4 EMU/Slit [7]. In the Linac 4 EMU, the irradiation conditions are very demanding with an proton energy 3 times higher than in ESS MEBT (12 MeV vs. 3.63 MeV) and smaller beam sizes. These high demanding conditions require of inclined surfaces in order to withstand irradiation. For Linac 4 EMU/Slit the graphite plate are therefore inclined 15º with respect to the beam. Even with beam inclination the temperature variation during the irradiation pulse is on the order of 1000 K [7].

Regarding the energy deposition, in Figure 16 we show the stopping power as function of depths for 3.63 MeV and 12 MeV. We observe how the penetration depths for 12 MeV at 15º is up to ~400 μm with stopping powers of 620 MeV/cm, while perpendicular irradiation with 3.63 MeV is up to 140 μm with stopping powers of ~760 MeV/cm.

In Table 11 we compare the operational parameters in the ESS MEBT and Linac 4 EMU/Slit. The surface load in Linac 4 is around twice higher than in the ESS MEBT, while the volumetric heat load in the Bragg peak are comparable on both cases. The higher energy fluxes in Linac 4, lead to higher temperature and stresses, around two times higher than for ESS MEBT. We have compared the thermomechanical response in both scenarios using a 1D FEM Model.

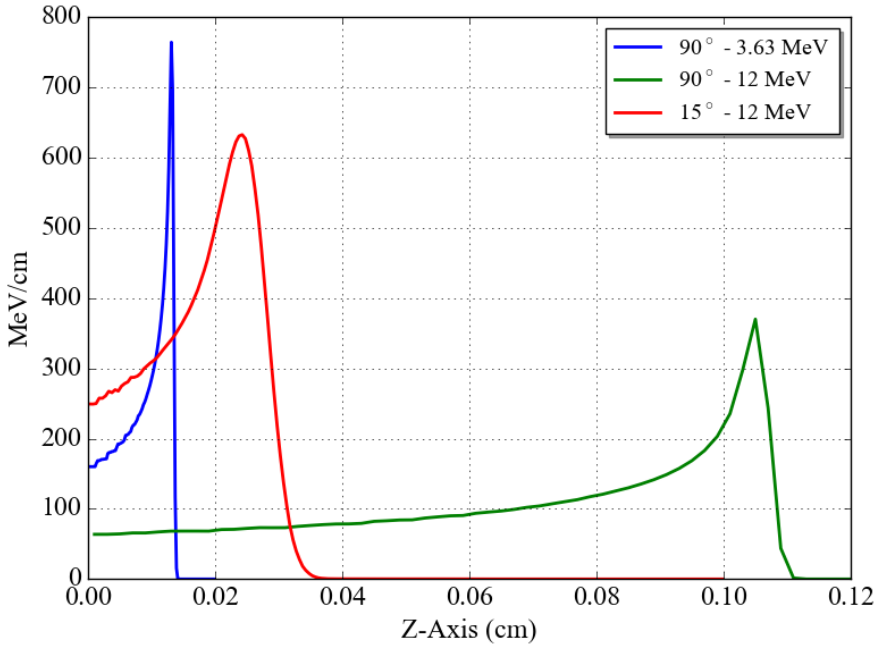

Figure 16: Stopping power for 3.63 MeV and 12 MeV protons in Graphite. Analysis done using MCNPX.

Table 11: Comparison of EMU/Slit irradiation parameters in ESS MEBT and Linac 4 [7].

		ESS MEBT EMU/Slit	**Linac4: Slit DTL 1m**
Material		Graphite	
Angle (°)		90	15
E (MeV)		3.63	12
Peak Current (mA)		62.5	65
Pulse duration (μs)		50	100
Beam size (mm)	σ_x	3.2	1.8
	σ_y	3.8	2.7
Beam Power (kW)		227	780
		Surface Load	
I'' (mA/cm^2)		82.16	55.09
I'' (μC/cm^2-pulse)		4.1	5.5
P (MW cm^{-2})		0.30	0.66
E (J cm^{-2})		15	66
		Peak Volumetric Load	
S (MeV/cm)		760	620
P (MW cm^{-3})		62	34
E (J cm^{-3})		3122	3416
		1D FEM Model	
ΔT (K)		555	1151
$\sigma_{Eq.}$ (MPa)		37	92

E.1 1D FEM Model

We use a 1D Ansys FEM model applying plane strain conditions in order to simulate thermomechanical effects of irradiation.

Regarding thermal conditions, we apply a uniform initial temperature of 300 K, the thermal load is either introduced as volumetric load and no radiative effects are included. For the geometry of the model a plate of 3 mm of thickness with a mesh with sizes from 2-10 μm is used.

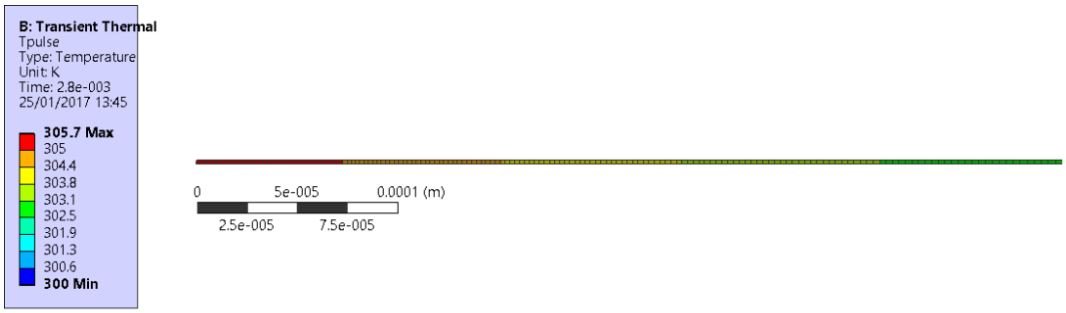

Figure 17: 1D FEM model for the estimation of the thermomechanical effects of the irradiation pulse. The Figure shows the temperature for an example for a pulse of 2.8 ms with powers of 3.54 MW/m^2 on copper.

References

[1] B. Cheymol and R. Miyamoto, “Preliminary design of the ESS slit and grid system,” Internal ESS ESS-0020535-V1.1, juillet 2015.

[2] B. Cheymol, E. Bravin, and D. Gerard, “Design of the Emittance Meter for the 3 and 12 MeV LINAC4 H-Beam,” *Energy MeV*, vol. 3, no. 3, p. 12, 2010.

[3] B. Cheymol, “Development of beam transverse profile and emittance monitors for the CERN LINAC4,” phdthesis, Université Blaise Pascal - Clermont-Ferrand II, 2011.

[4] Z. Izaola, “Emittance Unit Meter: Preliminary Design Review,” Jul-2016.

[5] T. Mora, I. Bustinduy, and F. Sordo, “ESS-Bilbao Beam Stoppers criteria (MEBT-BI-FC04-02),” 16-May-2016.

[6] M. Munoz, M. Eshraqi, A. Jansson, S. Molloy, and M. Lindroos, “Description of Modes for ESS Accelerator Operation,” Internal ESS ESS-0038258 Rev. 3 Prelminary State, Nov. 2015.

[7] F. Carra and A. Dallochio, “LINAC4 3MeV test stand: Thermo-mechanical analysis of the Slit,” CERN, CERN CH1211 Geneva 23 Switzerland, CERN Internal Report 1102149 0.1, Nov. 2010.

[8] SGL Group: The Carbon Company, “Specialty Graphites for the Metal Industry,” SGL Group, Commercial Brochure.

[9] F. P. Incropera, D. P. DeWitt, T. L. Bergman, and A. S. Lavine, *Fundamentals of Heat and Mass Transfer*, Edición: 6th ed. Hoboken, NJ: Wiley John + Sons, 2006.

[10] Y. Lee and M. Hartl, “ESS Target Materials Handbook,” Internal ESS ESS-0028465, Feb. 2016.

[11] ASM, Ed., *ASM andbook Volume 1: Properties and Selection: Irons, Steels, and High-Performance Alloys*, 10 edition. Materials Park: ASM International, 1990.

[12] S. Song and M. Yovanovich, “Explicit relative contact pressure expression - Dependence upon surface roughness parameters and Vickers microhardness coefficients,” 1987.

[13] ASM, *ASM Handbook Volume 2: Properties and Selection : Nonferrous Alloys and Special-Purpose Materials*, 10th edition. Place of publication not identified: ASM International, 1990.

[14] M. M. Yovanovich, J. R. Culham, and P. Teertstra, “Calculating interface resistance,” *Electron. Cool.*, vol. 3, no. 2, pp. 24–29, 1997.

[15] A. K. Hasselström and U. E. Nilsson, “Thermal contact conductance in bolted joints,” 2012.

[16] M. M. Yovanovich, “Micro and Macro Hardness Measurements, Correlations, and Contact Models,” presented at the 44th AIAA Aerospace Sciences Meeting and Exhibit, Reno, Nevada, 2006, vol. AIAA 2006-979.

[17] M. Bahrami, J. R. Culham, and M. M. Yovanovich, “Modeling Thermal Contact Resistance: A Scale Analysis Approach,” *J. Heat Transf.*, vol. 126, no. 6, pp. 896–905, Jan. 2005.

[18] P. Zhang, S. X. Li, and Z. F. Zhang, “General relationship between strength and hardness,” *Mater. Sci. Eng. A*, vol. 529, pp. 62–73, Nov. 2011.

[19] E. J. Pavlina and C. J. V. Tyne, “Correlation of Yield Strength and Tensile Strength with Hardness for Steels,” *J. Mater. Eng. Perform.*, vol. 17, no. 6, pp. 888–893, Apr. 2008.

[20] DIN51917, “Rockwell hardness of carbonaceous materials by the steel ball indentation method.” DIN, 1997.

[21] F. White, *Fluid Mechanics*, 7 edition. New York, N.Y.: McGraw-Hill Education, 2010.